REPORT SD-TR-89-47

(4)

AD-A210 613

Multiline Multimode CW Chemical Laser Performance

Prepared by

H. MIRELS
Aerophysics Laboratory
Laboratory Operations
The Aerospace Corporation
El Segundo, CA 90245

1 July 1989

Prepared for

SPACE SYSTEMS DIVISION
AIR FORCE SYSTEMS COMMAND
Los Angeles Air Force Base
P.O. Box 92960
Los Angeles, CA 90009-2960

This report was submitted by The Aerospace Corporation, El Segundo, CA 90245, under Contract No. F04701-85-C-0086-P00019 with the Space Systems Division, P. O. Box 92960, Los Angeles, CA 90009-2960. It was reviewed and approved for The Aerospace Corporation by W. P. Thompson, Director, Aerophysics Laboratory. Capt Scott W. Levinson was the project officer.

This report has been reviewed by the Public Affairs Office (PAS) and is releasable to the National Technical Information Service (NTIS). At NTIS, it will be available to the general public, including foreign nationals.

This technical report has been reviewed and is approved for publication. Publication of this report does not constitute Air Force approval of the report's findings or conclusions. It is published only for the exchange and stimulation of ideas.

SCOTT W. LEVINSON, CAPT, USAF
Project Officer
SSD/CNID

JAMES A. BERES, LT COL, USAF
Director, AFSTC/WCO OL-AB

UNCLASSIFIED

SECURITY CLASSIFICATION OF THIS PAGE

REPORT DOCUMENTATION PAGE

1a. REPORT SECURITY CLASSIFICATION Unclassified	1b. RESTRICTIVE MARKINGS
2a. SECURITY CLASSIFICATION AUTHORITY	3. DISTRIBUTION/AVAILABILITY OF REPORT Approved for public release; distribution unlimited.
2b. DECLASSIFICATION/DOWNGRADING SCHEDULE	
4. PERFORMING ORGANIZATION REPORT NUMBER(S) TR-0088(3907)-1	5. MONITORING ORGANIZATION REPORT NUMBER(S) SD-TR-89-47
6a. NAME OF PERFORMING ORGANIZATION The Aerospace Corporation Laboratory Operations 6b. OFFICE SYMBOL (If applicable)	7a. NAME OF MONITORING ORGANIZATION Space Systems Division
6c. ADDRESS (City, State, and ZIP Code) El Segundo, CA 90245	7b. ADDRESS (City, State, and ZIP Code) Los Angeles Air Force Base Los Angeles, CA 90009-2960
8a. NAME OF FUNDING/SPONSORING ORGANIZATION 8b. OFFICE SYMBOL (If applicable)	9. PROCUREMENT INSTRUMENT IDENTIFICATION NUMBER F04701-85-C-0086-P00019
8c. ADDRESS (City, State, and ZIP Code)	10. SOURCE OF FUNDING NUMBERS PROGRAM ELEMENT NO / PROJECT NO. / TASK NO / WORK UNIT ACCESSION NO.

11. TITLE (Include Security Classification)

Multiline Multimode CW Chemical Laser Performance

12. PERSONAL AUTHOR(S)

Mirels, Harold

13a. TYPE OF REPORT	13b. TIME COVERED	14. DATE OF REPORT (Year, Month, Day)	15. PAGE COUNT
	FROM ____ TO ____	1 July 1989	40

16. SUPPLEMENTARY NOTATION

17. COSATI CODES			18. SUBJECT TERMS (Continue on reverse if necessary and identify by block number)
FIELD	GROUP	SUB-GROUP	cw chemical laser; Nonequilibrium Effects
			Multiline Laser; Theoretical Performance
			Multimode Laser

19. ABSTRACT (Continue on reverse if necessary and identify by block number)

Effects of translational and rotational nonequilibrium on large scale cw chemical laser performance are evaluated for the case of a Fabry-Perot resonator with multiple longitudinal modes. Numerical results are presented for the limit $\Delta\nu_c << \Delta\nu_h << \Delta\nu_d$, where $\Delta\nu_c$, $\Delta\nu_h$, and $\Delta\nu_d$ denote longitudinal mode separation, homogeneous width, and Doppler width, respectively. Results include the effect of threshold gain on the power in each longitudinal mode, the power associated with each rotational energy level, and the net laser power. In the case of a saturated laser, an increase of threshold gain results in an increase in the output from strong rotational transitions at the expense of the output from weak rotational transitions. Total output is reduced. With further increase of threshold gain, the output from all rotational transitions is reduced. The case of rotational nonequilibrium and translational equilibrium is also considered. The latter case, a common assumption, is shown to provide net output power that is intermediate between the values for rotational and translational equilibrium and for rotational and translational nonequilibrium.

20. DISTRIBUTION/AVAILABILITY OF ABSTRACT ☐ UNCLASSIFIED/UNLIMITED ☒ SAME AS RPT ☐ DTIC USERS	21. ABSTRACT SECURITY CLASSIFICATION Unclassified
22a. NAME OF RESPONSIBLE INDIVIDUAL	22b. TELEPHONE (Include Area Code) / 22c. OFFICE SYMBOL

DD FORM 1473, 84 MAR — 83 APR edition may be used until exhausted. All other editions are obsolete

SECURITY CLASSIFICATION OF THIS PAGE

UNCLASSIFIED

CONTENTS

FIGURES

TABLES

I. INTRODUCTION

Continuous wave (cw) chemical lasers are inhomogeneously broadened. Under lasing conditions, the gain medium is in a state of both rotational and translational nonequilibrium.

Early cw chemical laser models incorporated the assumption of rotational and translational equilibrium and gave reasonable estimates of net laser output power and scaling laws (e.g., Refs. 1 and 2). The later inclusion of rotational nonequilibrium in these models provided estimates of the output from various rotational energy levels (e.g., Refs. 3-5). The inclusion of translational nonequilibrium (i.e., inhomogeneous broadening with hole burning) provided estimates of the output from each of the multiple longitudinal modes in large scale cw chemical lasers (e.g., Refs. 6-8).

The simultaneous consideration of both rotational and translational nonequilibrium in cw chemical lasers has received less attention. A general analytic model[9] and a computer code[10,11] have been developed with limited results presented. More recently, an analytic model was developed[12] that provides solutions for both amplifiers and Fabry-Perot (F-P) oscillators.

The purpose of the present report is to consider both rotational and translational nonequilibrium and provide a multiline (multiple rotational energy levels) and multimode (multiple longitudinal modes) solution for a large scale cw chemical laser with an F-P resonator. It is assumed that $\Delta\nu_c \ll \Delta\nu_h \ll \Delta\nu_d$, where $\Delta\nu_c$, $\Delta\nu_h$, and $\Delta\nu_d$ are frequencies that characterize longitudinal mode separation, homogeneous width, and Doppler width, respectively. The present report may be viewed as an application of Ref. 12 that generalizes Ref. 7 to include multiple rotational energy levels. The notation is the same as that in Ref. 12. Symbols and nondimensional variables are summarized in Appendixes A and B, respectively. The corresponding case of rotational nonequilibrium and translational equilibrium is discussed in Appendix C.

II. THEORY

The present model is briefly described. Laser equations are formulated, and solutions are then presented for a cw chemical laser oscillator with laminar mixing.

A. FLOW MODEL

A cw chemical laser with an F-P resonator is illustrated in Fig. 1a. The present simplified mixing model is illustrated in Fig. 1b. The reactants are assumed to be premixed but do not react until a flame sheet, $y_f(x)$, is reached. The flame sheet shape is specified, a priori, from diffusion theory. The streamwise station where the flame sheet reaches the channel center line is denoted x_D and characterizes the diffusion rate. The width per semichannel and the number of semichannels are denoted w and n_{sc}, respectively. Laser radiation is in the $\pm y$ direction.

B. GAIN AND RESONATOR MODEL

In order to simplify the mathematical development, we assume a "Q" type laser transition

$$v + 1, J \rightarrow v, J \qquad (1a)$$

rather than the "P" type laser transition

$$v + 1, J - 1 \rightarrow v, J \qquad (1b)$$

appropriate for cw chemical lasers. Here, v, J denotes vibrational and rotational energy level, respectively. This Q type laser transition approximation is used in Ref. 11 and is consistent with other simplifying assumptions used in the present model. In addition, we consider a two-vibrational energy level model and denote the upper and lower levels by subscripts 2 and 1, respectively. Expressions for gain are given by Eqs.

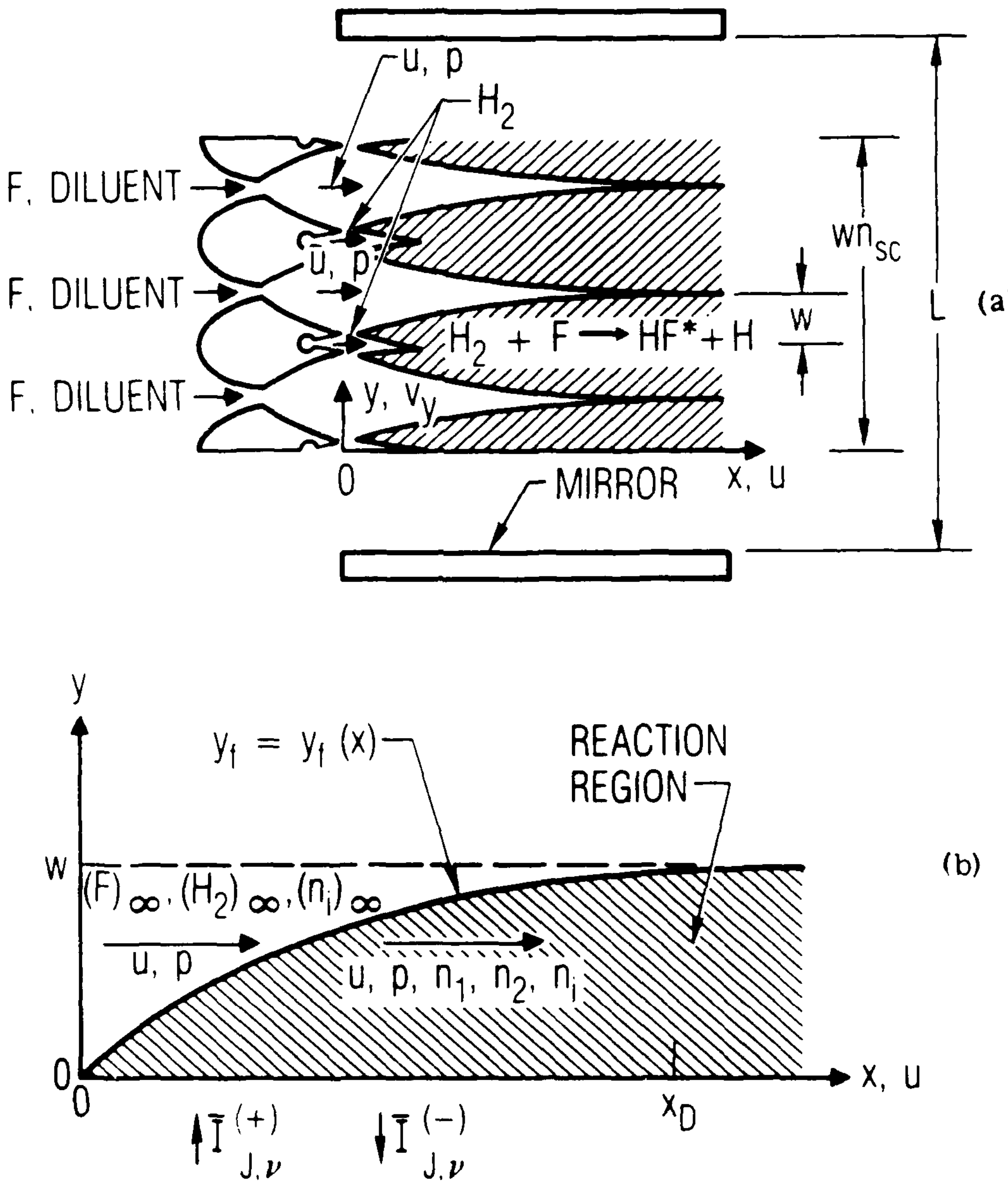

Fig. 1. Continuous Wave Chemical Laser (a) Flow Field and F-P Resonator and (b) Flame Sheet Model of Reaction Zone [1,6-8]

(B-5a)-(B-5d). The quantity $n_v(J,\nu)$, in these equations, denotes the number density of particles in the v, J level that are resonant with radiation in the frequency range ν to $\nu + d\nu$. (In the present study, as in the previous studies,[6,12] resonant frequency is used instead of particle thermal velocity in order to evaluate the interaction of the radiation field with the inhomogeneously broadened gain medium. For radiation in the ± y direction, the resonant frequency ν is related to the particle thermal velocity v_y by the Doppler relation $(\nu/\nu_o) - 1 = \mp v_y/c$. Similarly, $n_v(J)$ and n_v denote the net number density of particles in the energy levels v, J, and v, respectively. For the case of translational and rotational equilibrium, the quantities, $n_v(J,\nu)$, $n_v(J)$, and n_v are related by Eqs. (B-4a)-(B-4d). Note from Eq. (B-4d) that $\bar{f}_J$ denotes the fraction of particles in rotational level J for the case of rotational equilibrium. The maximum value of $\bar{f}_J$ is denoted $\bar{f}_{J,m}$ and is a function of $Q_R = T_R/T$ (Table I). It is convenient to let $\bar{f}_r = \bar{f}_{J,m}$, where $\bar{f}_r$ is the reference value of $\bar{f}_J$ used in the normalizations in Eqs. (B-3a)-(B-3d).

The two end mirrors in the F-P resonator are each assumed to have the same reflectivity, R_m. Line center laser frequency is denoted ν_o [e.g., Eq. (B-4c)], and the dependence on J is ignored. The mirror separation L is adjusted so that the longitudinal mode frequencies $\nu_{J,j}$ are symmetric about ν_o. The longitudinal mode frequencies are then

$$\nu_{J,j} = \nu_o + j\,\Delta\nu_c \qquad j = 0, \pm 1, \pm 2, \ldots \qquad (2a)$$

or

$$\nu_{J,j} = \nu_o + (j - \tfrac{1}{2})\Delta\nu_c \qquad j = 1, 2, 3, \ldots \qquad (2b)$$

$$= \nu_o + (j + \tfrac{1}{2})\Delta\nu_c \qquad j = -1, -2, -3, \ldots$$

where j and $\Delta\nu_c$ denote longitudinal mode number and longitudinal separation, respectively. Let $\bar{I}_{J,j}^{(+)}$ and $\bar{I}_{J,j}^{(-)}$ denote local radiation intensity in the +y and -y directions (Fig. 1b). Due to the symmetry of the longi-

TABLE I. Maximum value of $\bar{f}_J$ and corresponding value of J for fixed θ_R.[a]

θ_R	J_m	$\bar{f}_{J,m}$
1/10	2	0.2654
1/20	3	0.1889
1/40	4	0.1353
1/60	5	0.1106
1/80	6	0.0957
1/100	7	0.0854

[a] Eq. (B-4d).

tudinal modes about ν_o, the interaction of $\bar{I}_{J,j}^{(+)}$ and $\bar{I}_{J,j}^{(-)}$ with the gain medium can be evaluated by consideration of the net local intensity $\bar{I}_{J,j} = \bar{I}_{J,j}^{(+)} + \bar{I}_{J,j}^{(-)}$, as discussed in Ref. 6. A typical variation of local intensity with frequency is illustrated in Fig. 2. Here, $\nu_{J,f}$ denotes the highest frequency at which lasing occurs.

C. LASER EQUATIONS

Consider the case

$$R_t \gg 1; \; R_r \gg 1 \tag{3a}$$

$$\frac{\Delta\nu_h}{\Delta\nu_d} \sim \frac{p(\mathrm{Torr})}{100} \ll 1 \tag{3b}$$

$$\frac{\Delta\nu_c}{\Delta\nu_h} \sim \frac{50}{L(m)\,p(\mathrm{Torr})} \ll 1 \tag{3c}$$

$$\left| 1 - \frac{R_t}{R_r} \right| \frac{\Delta\nu_h}{\Delta\nu_d} \ll 1 \tag{3d}$$

where L(m) is resonator mirror separation in meters, p(Torr) is gain region pressure in Torr, and where $R_t = k_{tr}/k_{cd}$ and $R_r = k_{rr}/k_{cd}$ denote the ratio of the translational and rotational relaxation rate to the rate of collisional deactivation. In general, $R_t/R_r = 0(1)$ in cw chemical lasers.[12] Equations (3b) and (3c) imply multiple longitudinal modes. These equations apply for large scale chemical lasers[6,7] (e.g., p = 10 Torr, L = 50 m) and are illustrated in Fig. 3. As a consequence of Eqs. (3a) and (3d), the equations that define the performance of a cw chemical laser with an F-P resonator are[12]

$$\frac{N_{J\nu}^{-}}{f_J e^{-X^2} N^{-}} = \frac{1 + 0\left\{[1 - (R_t/R_r)](\Delta\nu_h/\Delta\nu_d)\right\}}{1 + \sum_j L(\nu - \nu_{J,j}) I_{J,j}} \tag{4a}$$

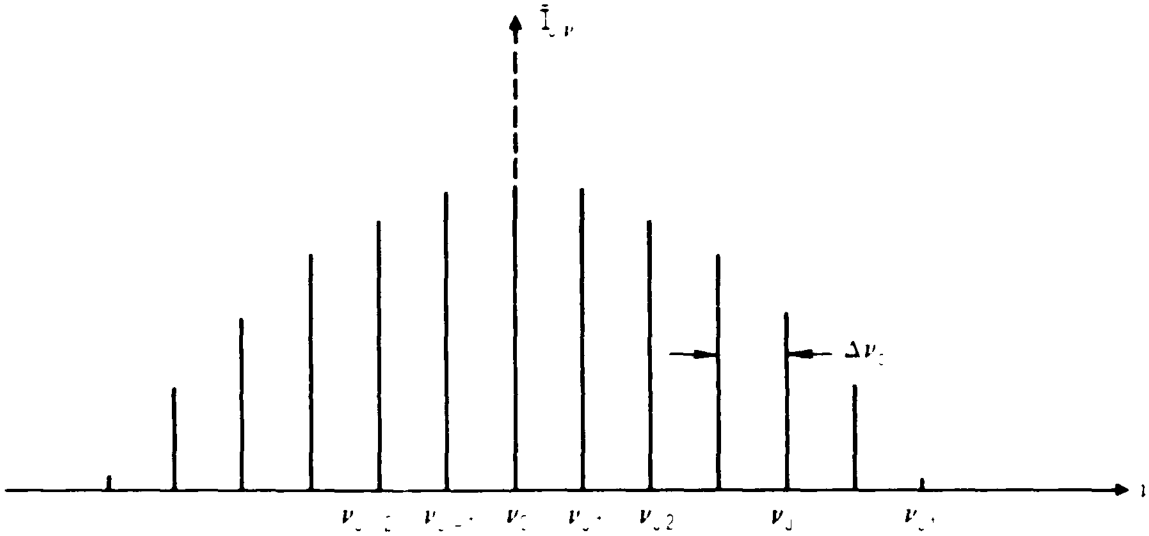

Fig. 2. Local Longitudinal Mode Intensity in F-P Resonator for Case Where $\nu_{J,j}$ Is Symmetric About ν_o.
Note: $\bar{I}_{J,\nu} = \bar{I}_{J,\nu}^{(+)} + \bar{I}_{J,j}^{(-)}$ [Eq. (2a)].

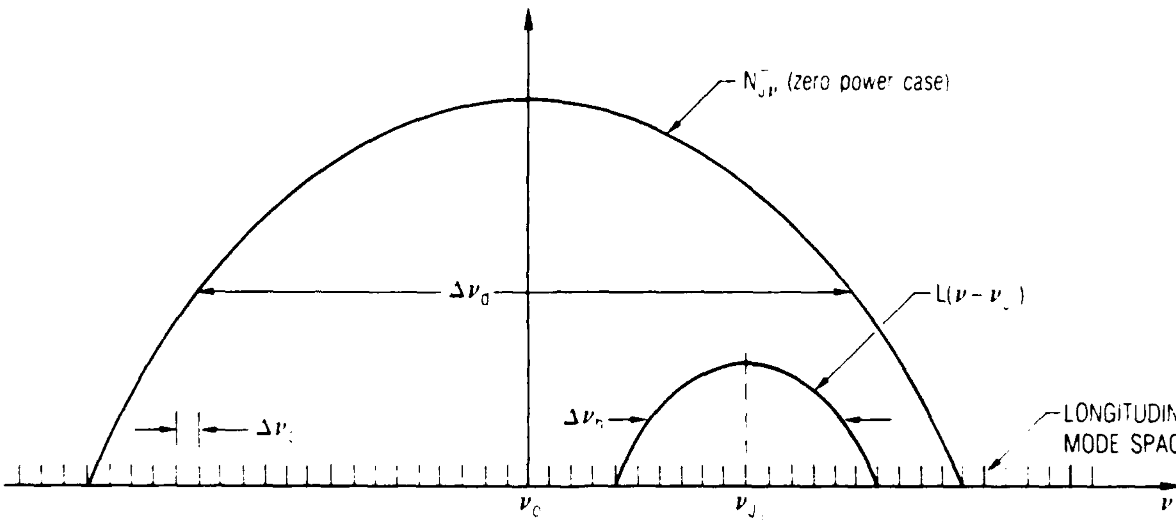

Fig. 3. Characteristic Frequencies

$$dN^-/d\zeta = dN_T/d\zeta - N_T - N^- - (SG_c/\pi) \sum_J \sum_j I_{J,j} \quad (4b)$$

$$G_J(\nu') = \int_{-\infty}^{\infty} N_{J\nu}^- \, L(\nu - \nu') \, \frac{d\nu}{\Delta\nu_h} \quad (4c)$$

where G_c is the threshold gain, and other variables are defined in Appendixes A and B. These equations can be evaluated without consideration of N_J^-, which is found from

$$\frac{N_J^-}{f_J N^-} = 1 - \left(\frac{4\ell n2}{\pi}\right)^{1/2} \frac{\Delta\nu_h}{\Delta\nu_d} \frac{R_t}{R_r} \frac{G_c}{f_J N^-} \sum_j I_{J,j} \quad (4d)$$

Here, $N_{J\nu}^-$, N_J^-, N^-, N_T, and $I_{J,j}$ are normalized forms of the variables $n_2(J,\nu) - n_1(J,\nu)$, $n_2(J) - n_1(J)$, $n_2 - n_1$, $n_2 + n_1$, and $\bar{I}_{J,j}$, respectively. The quantity $\bar{I}_{J,j}$ has been normalized by a saturation intensity, $\varepsilon_r k_{tr}/(2\bar{\sigma}_r)$, which characterizes hole burning (translational nonequilibrium) effects. When $I_{J,j}$ is small, the laser medium is in translational and rotational equilibrium. Equations (1a) and (1d) then indicate

$$\frac{N_{J\nu}^-}{f_J e^{-X^2} N^-} = \frac{N_J^-}{f_J \, N^-} = 1 \quad (5)$$

When $I_{J,j}$ is not small, a nonequilibrium solution of Eqs. (4a)-(4d) is required.

Equation (3c) indicates that there are many longitudinal modes within the homogeneous width $\Delta\nu_h$. In order to facilitate the summation of $I_{J,j}$ $L(\nu - \nu_{J,j})$ in Eq. (4a), it is convenient to replace $I_{J,j}$ by a continuous distribution $\tilde{I}_J(\nu)$ in the interval from $\nu_{J,j} - \Delta\nu_c/2$ to $\nu_{J,j} + \Delta\nu_c/2$. Thus

$$I_{J,j} \equiv \int_{\nu_{J,j} - \Delta\nu_c/2}^{\nu_{J,j} + \Delta\nu_c/2} \tilde{I}_J(\nu) d\nu = \tilde{I}_J(\nu_{J,j})\Delta\nu_c \quad (6)$$

It follows that

$$\sum_j I_{J,j}\, L(\nu - \nu_{J,j}) = \int_{-\infty}^{\infty} \tilde{I}_J(\nu_{J,j})\, L(\nu - \nu_{J,j})d\nu_{J,j} \tag{7a}$$

$$= (\pi/2)\Delta\nu_h \tilde{I}_J(\nu)$$

$$I_J = \sum_j I_{J,j} = \int_{-\infty}^{\infty} \tilde{I}_J(\nu)d\nu \tag{7b}$$

$$I = \sum_J I_J \tag{7c}$$

Let X_{Jf} denote the largest lasing frequency for a given J. For the present case of an F-P resonator with closely packed longitudinal modes (e.g., $\Delta\nu_c << \Delta\nu_h$), it is expected that $N^-_{J\nu}$ will depart only slightly from the threshold value $N^-_{J\nu_i}$ for frequencies in the range $|X| \leq X_{Jf}$ (Fig. 4). The resulting particle density distribution can then be approximated by

$$N^-_{J\nu}/N^-_{J\nu_i} = 1 \qquad |X| \leq X_{Jf} \tag{8a}$$

$$= e^{X^2_{Jf} - X^2} \qquad |X| > X_{Jf} \tag{8b}$$

which assumes that $N^-_{J\nu}$ is continuous at $|X| = X_{Jf}$ and has an equilibrium distribution for $|X| > X_{Jf}$. Substitution of Eqs. (8a)-(8b) into Eqs. (4a)-(4d) and (7a)-(7c) yields

$$(2/\pi)G_c = N^-_{J\nu_i} \tag{9a}$$

$$(\pi/2)\Delta\nu_h\, \tilde{I}_J(\nu) = e^{X^2_{Jf} - X^2} - 1 \qquad |x| \leq X_{Jf} \tag{9b}$$

$$(\pi \ell n2)^{1/2}\, (\Delta\nu_h/\Delta\nu_d)I_J = e^{X^2_{Jf}} \text{erf}\, X_{Jf} - (2/\pi^{1/2})X_{Jf} \tag{9c}$$

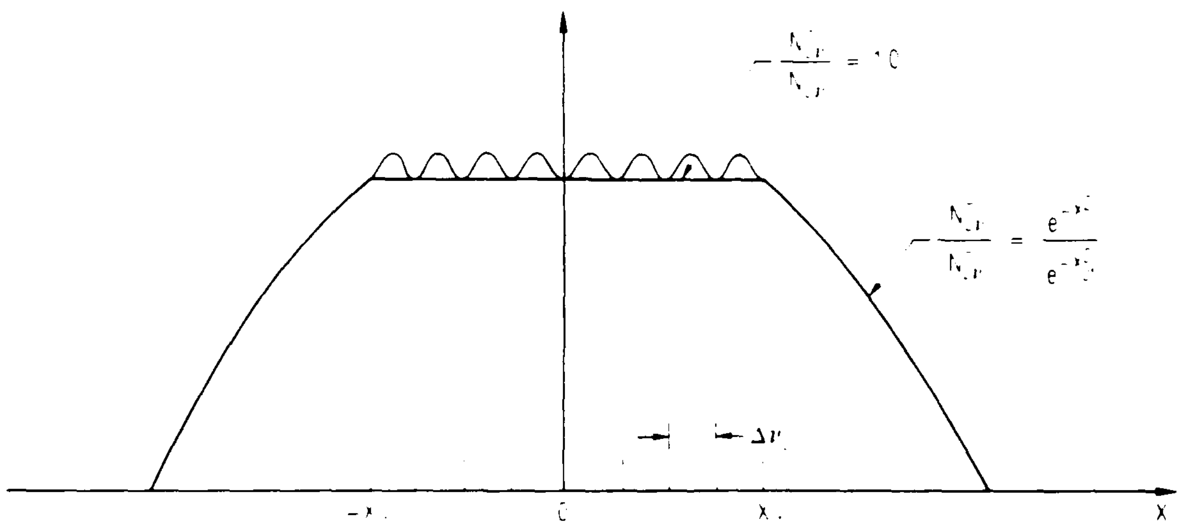

Fig. 4. Variation of Inversion Number Density with Frequency for F-P Resonator with $\Delta\nu_c \ll \Delta\nu_h \ll \Delta\nu_d$

$$X_{Jf}^2 = \ln \left[\frac{f_J N^-}{(2/\pi)G_c}\right] \qquad (9d)$$

where it is assumed, in Eqs. (9b) and (9d), that $\Upsilon_J = 0$ at $|X| = X_{Jf}$. Equation (9b) indicates an exponential variation of $\Upsilon_J(\nu)$ with X.

Output power per unit volume is found from [e.g., Eq. (B-6c)]

$$dP_J(\nu)/d\zeta = [SG_c/(2\pi)]\Upsilon_J(\nu) \qquad (10a)$$

$$dP_J/d\zeta = [SG_c/(2\pi)]I_J = \int_{-\infty}^{\infty} P_J(\nu)d\nu \qquad (10b)$$

$$dP/d\zeta = \sum_J dP_J/d\zeta \qquad (10c)$$

Integration of Eqs. (10a)-(10c) to the end of the lasing region ζ_e provides the corresponding net output values $[P_J(\nu)]_e$, $P_{J,e}$, and P_e.

D. LAMINAR MIXING

For the case of laminar mixing[6,12]

$$N_T = (\zeta/\zeta_D)^{1/2}$$

Eq. (4b) may be expressed in the form

$$z_D(dN^-/dz) = 1 - 2z_D z N^- - 2z^2 - 2z\phi_t \sum_J (\pi \ln 2)^{1/2}(\Delta\nu_h/\Delta\nu_d)I_J \qquad (11)$$

where

$$z = \zeta^{1/2};\ z_D = \zeta_D^{1/2} \qquad (12a)$$

$$\phi_t = (2/\pi)z_D G_c \bar{f}_r R_t \qquad (12b)$$

Integration of Eq. (11) for the case of zero power yields

$$z_D N^- = 2D(z) - z \tag{12c}$$

where

$$D(z) \equiv e^{-z^2} \int_0^z e^{t^2} dt \tag{12d}$$

is the Dawson integral.[13] Let subscript i denote conditions at the station where lasing is initiated. The boundary condition at this station is

$$z_D N_i^- = (2/\pi) z_D G_c / f_{J,m} = 2D(z_i) - z_i \tag{13}$$

where $f_{J,m}$ denotes the maximum value of f_J. Corresponding values of z_i, $z_D N_i^-$, and $(2/\pi) z_D G_c / f_{J,m}$ are listed in Table II and are used interchangeably. It is convenient to choose $\bar{f}_r = \bar{f}_{J,m}$, so that $f_{J,m} = 1$. However, for generality, $f_{J,m}$ will be retained in subsequent equations. The integration of Eq. (11), subject to the boundary conditions given by Eq. (13), is now discussed for equilibrium and nonequilibrium cases.

1. EQUILIBRIUM ($R_t \to \infty$, $R_r \to \infty$)

In the limit of translational and rotational equilibrium ($R_1 \to \infty$, $R_r \to \infty$), $X_{Jf} \to 0$ and lasing occurs on line center at the single rotational level corresponding to the maximum value of f_J. Thus, in the region $z_i \leq z \leq z_e$

$$z_D N^- = z_D N_i^- = (2/\pi) z_D G_c / f_{J,m} \tag{14a}$$

$$2\phi_t (\pi \ell n 2)^{1/2} (\Delta\nu_h / \Delta\nu_d) I = (1 - 2 z z_D N_i^- - 2z^2)/z \tag{14b}$$

Also

$$z_i = 2D(z_i) - z_D N_i^- \tag{14c}$$

TABLE II. Relation between station where lasing is initiated z_i, threshold number density N_i^-, and threshold gain G_c for laminar mixing.[a]

z_i	$z_D N_i^- = \frac{z_D G_c}{(\pi/2) f_{J,m}}$
0.001	0.0010
0.005	0.0050
0.010	0.0100
0.050	0.0498
0.100	0.0987
0.200	0.1895
0.300	0.2653
0.400	0.3199
0.500	0.3489
0.552	0.3528[b]

[a](Eq. (13).

[b]Maximum zero power value.

$$2z_e = [(z_D N_i^-)^2 + 2]^{1/2} - z_D N_i^- \tag{14d}$$

$$2z_D P_e = \left[z - z^2 z_D N_i^- - (2/3)z^3\right]_{z_i}^{z_e} \tag{14e}$$

In the further limit $z_D N_i^- \to 0$,

$$z_i \to 0 \; ; \; z_e \to 2^{-1/2} \; ; \; z_D P_e \to (18)^{-1/2} \tag{15}$$

which corresponds to saturated laser operation.

2. NONEQUILIBRIUM ($R_t >> 1$, $R_r >> 1$)

Under conditions of translational and rotational nonequilibrium, a numerical integration of Eq. (11) is generally required.

For z near z_i, the last term in Eq. (11) is negligible, and the zero order solution is applicable. Thus the leading terms of the solution, near $z = z_i$, are

$$\frac{N^-}{N_i^-} - 1 = \left[\frac{1 - 4z_i D(z_i)}{2D(z_i) - z_i}\right](z - z_i) \tag{16a}$$

$$X_{Jf} = [(N^-/N_i^-) - 1]^{1/2} \qquad (f_J = f_{J,m}) \tag{16b}$$

Note that $(N^-/N_i^-) - 1$ has a linear dependence on $z - z_i$, while X_{Jf} varies as $(z - z_i)^{1/2}$.

In order to integrate Eq. (11), it is necessary to specify θ_R, $\bar{f}_r$, R_t, and z_i (or $Z_D N_i^-$). The following quantities can then be found:

$$z_D N_i^- = 2D(z_i) - z_i \tag{17a}$$

$$\phi_t = z_D N_i^- f_{J,m} \bar{f}_r R_t \tag{17b}$$

$$\frac{f_J}{f_{J,m}} = \frac{(2J + 1)\exp[-J(J + 1)\theta_R]}{(2J_m + 1)\exp[-J_m(J_m + 1)\theta_R]} \tag{17c}$$

The integration of Eq. (11) proceeds by the evaluation of

$$X_{Jf} = \{\ell n[f_J N^- /(f_{J,m} N_i^-)]\}^{1/2} \tag{17d}$$

$$(\pi \ell n_2)^{1/2}(\Delta\nu_h/\Delta\nu_d) I_J = e^{X_{Jf}^2} \operatorname{erf} X_{Jf} - (2/\pi^{1/2}) X_{Jf} \tag{17e}$$

at successive streamwise stations. The range of J, at each streamwise station, is limited by the requirement that X_{Jf} be real in Eq. (17d). Net output is found from Eqs. (10a)-(10c). Thus,

$$\Delta\nu_d z_D [P_J(\nu)]_e = 2\left(\frac{\ell n 2}{\pi}\right)^{1/2} \phi_t \int_o^{z_e} (e^{X_{Jf}^2 - X^2} - 1) z dz \tag{18a}$$

$$z_D P_{J,e} = \phi_t \int_o^{z_e} (e^{X_{Jf}^2} \operatorname{erf} X_{Jf} - \frac{2}{\pi^{1/2}} X_{Jf}) z dz \tag{18b}$$

$$z_D P_e = \sum_J z_D P_{J,e} \tag{18c}$$

where the integrands in Eqs. (18a) and (18b) are either nonnegative or zero. (That is, the effective integration interval in Eqs. (18a) and (18b) corresponds to values of z for which the integrand is nonnegative.)

III. NUMERICAL RESULTS AND DISCUSSION

Solutions of Eqs. (17) and (18) have been obtained for cases where

$$z_i = 0.001 - 0.5 \quad (19a)$$

$$Q_R = 1/80 \ (J_m = 6, \ f_{J,m} = 0.0957) \quad (19b)$$

$$f_r = f_{J,m} = 0.0957 \ (f_{J,m} = 1) \quad (19c)$$

$$R_t = 100 \quad (19d)$$

$$R_r >> 1 \quad (19e)$$

Results, which are presented in Figs. 5 to 8, are discussed herein.

Figure 5a indicates the variation of inversion number density $z_D N^-$ with streamwise distance in the lasing region $z_i \leq z \leq z_e$ for a variety of threshold gains. (Recall from Table II that z_i and $(2/\pi)2_D G_c$ are used interchangeably). The inversion number density $z_D N^-$ increases above the threshold value $z_D N_i^-$ for $z_i < z < z_e$. In the limit $R_t \rightarrow \infty$, $z_D N^- = z_D N_i^-$ in this region.

The variation of local laser intensity I_J with streamwise distance is given in Fig. 5b for the case $z_i = 0.1$. In accord with Eq. (19b), maximum intensity is obtained for J = 6. Note that for the present case of an F-P resonator, the peak intensity for each J level occurs at the same streamwise station. The streamwise extent of the lasing region decreases with departure of J from J = 6.

The number of longitudinal modes at a given streamwise station is approximately equal to $2 X_{Jf}/\Delta\nu_c$. The variation of X_{Jf} and, therefore, the variation of the number of longitudinal modes with streamwise distance, is given in Fig. 5c for $z_i = 0.1$. It is clear, from Figs. 5b and 5c, and from physical considerations, that X_{Jf} is a maximum where I_J is a maximum and that the streamwise extent of X_{Jf} is the same as that for I_J.

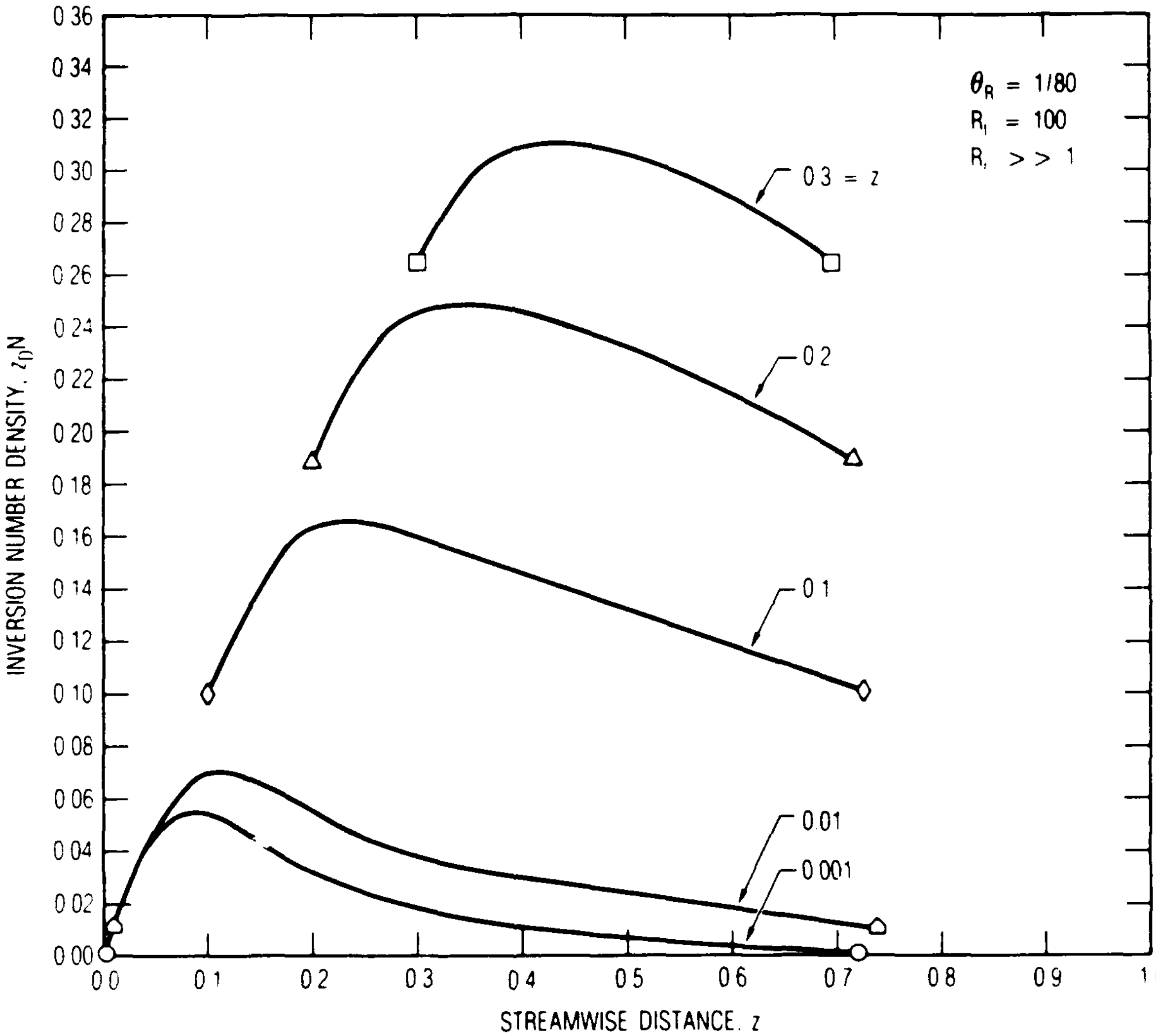

Fig. 5. Variation of Inversion Number Density, Laser Intensity, and Longitudinal Mode Frequency Range for F-P Resonator with Operating Conditions Given by Eq. (19). (a) Inversion number density in lasing region, $z_i \le z \le z_e$.

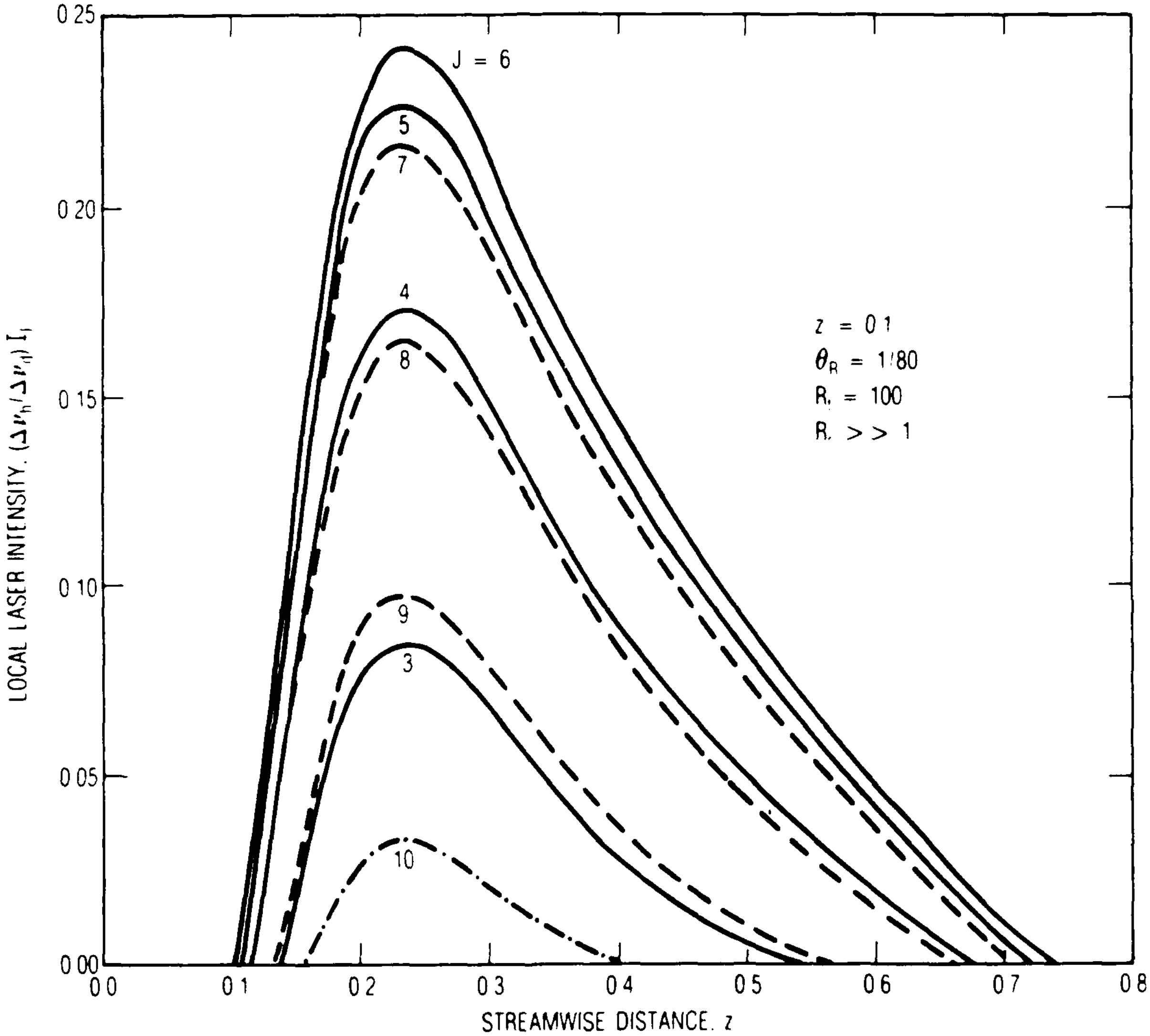

Fig. 5. Variation of Inversion Number Density, Laser Intensity, and Longitudinal Mode Frequency Range for F-P Resonator with Operating Conditions Given by Eq. (19). (b) Local laser intensity, z_i = 0.1.

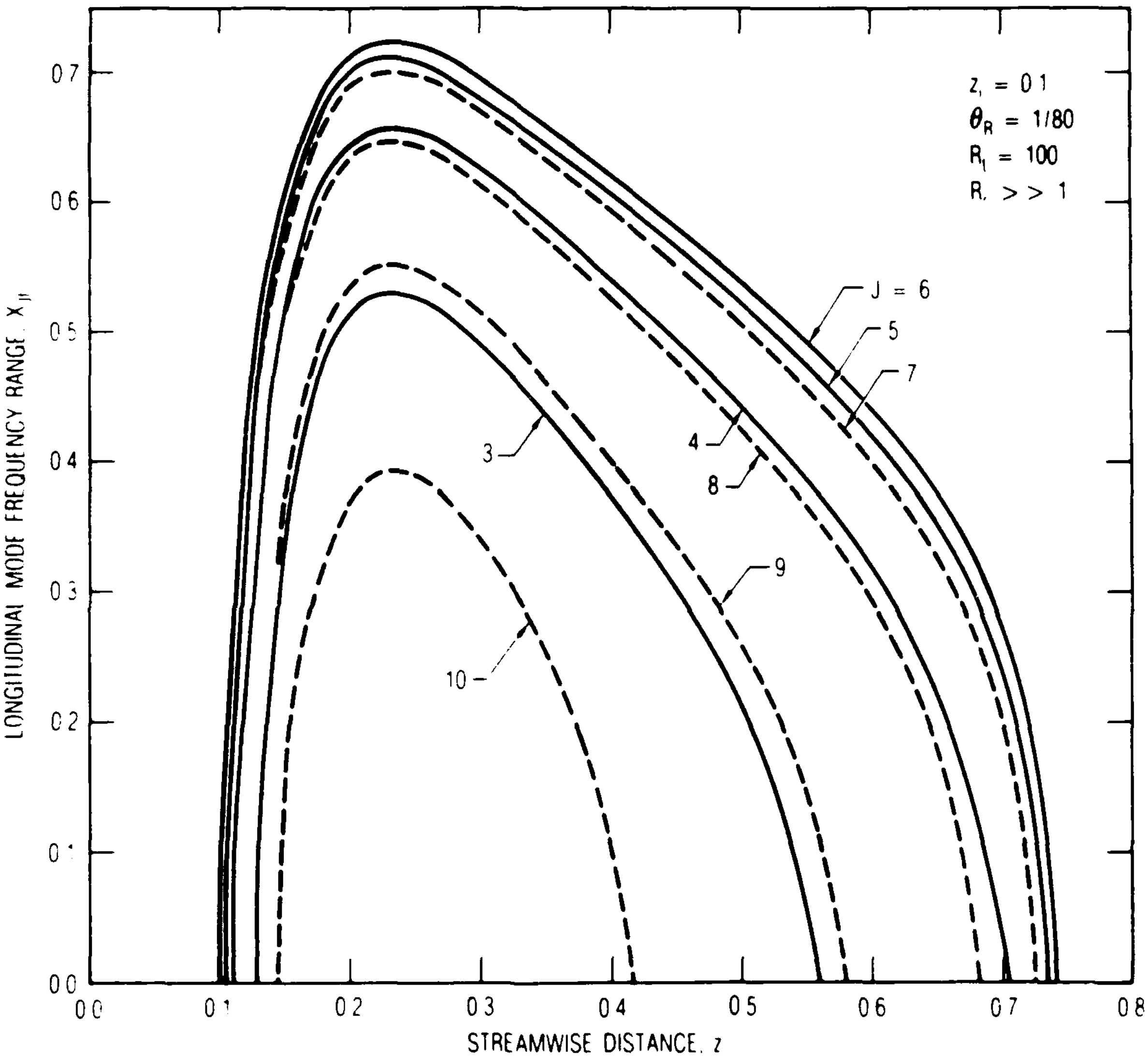

Fig. 5. Variation of Inversion Number Density, Laser Intensity, and Longitudinal Mode Frequency Range for F-P Resonator with Operating Conditions Given by Eq. (19). (c) Logitudinal mode frequency range, z_i = 0.1.

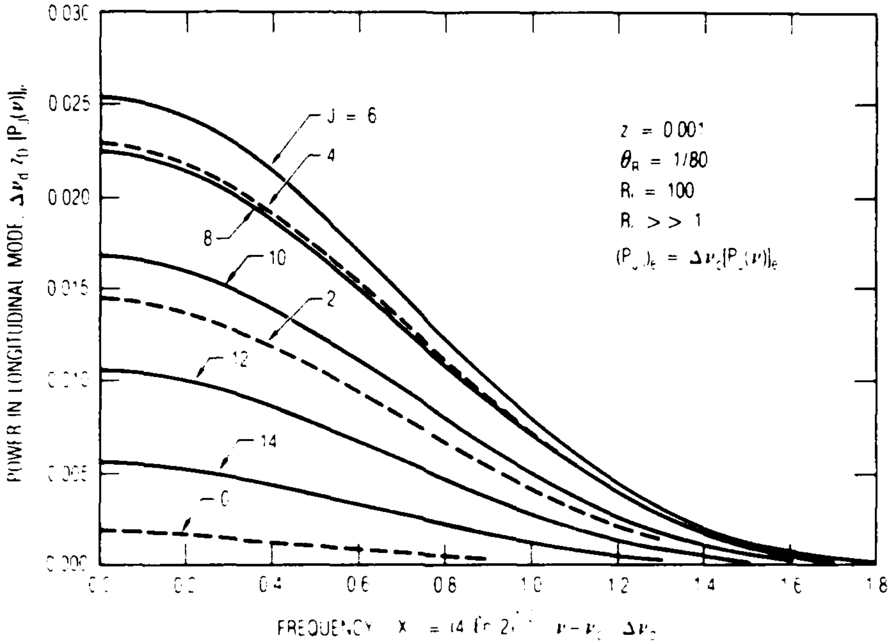

(a)

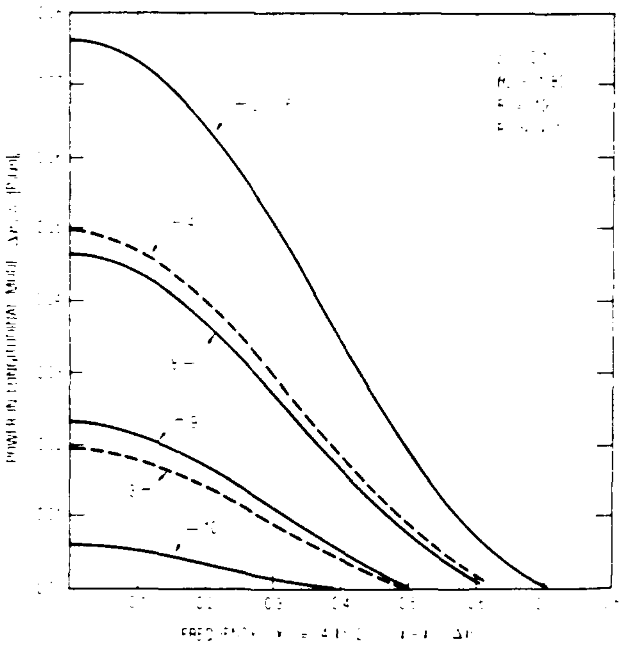

(b)

Fig. 6. Variation of Net Longitudinal Mode Output Power with Frequency for F-P Resonator with Operating Conditions Given by Eqs. (19a)-(19e). (a) Case z_i = 0.001 and (b) z_i = 0.1.

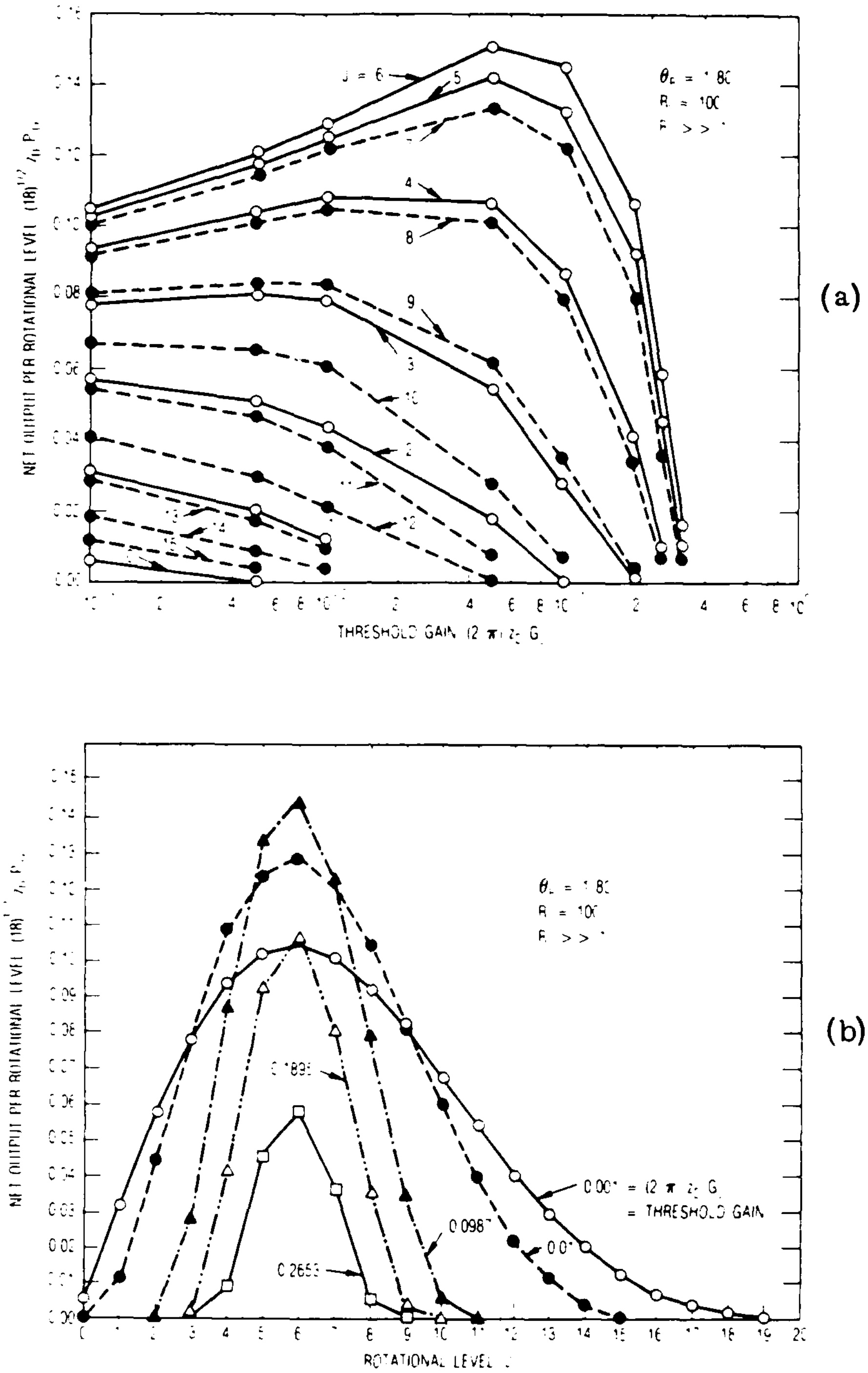

Fig. 7. Net Output Power from Each Rotational Level Versus (a) Threshold Gain Parameter $z_D N_i^-$ and (b) Rotational Level J for Operating Conditions Given by Eq. (19). Note that ordinate may be viewed as fraction of net output power from a saturated laser.

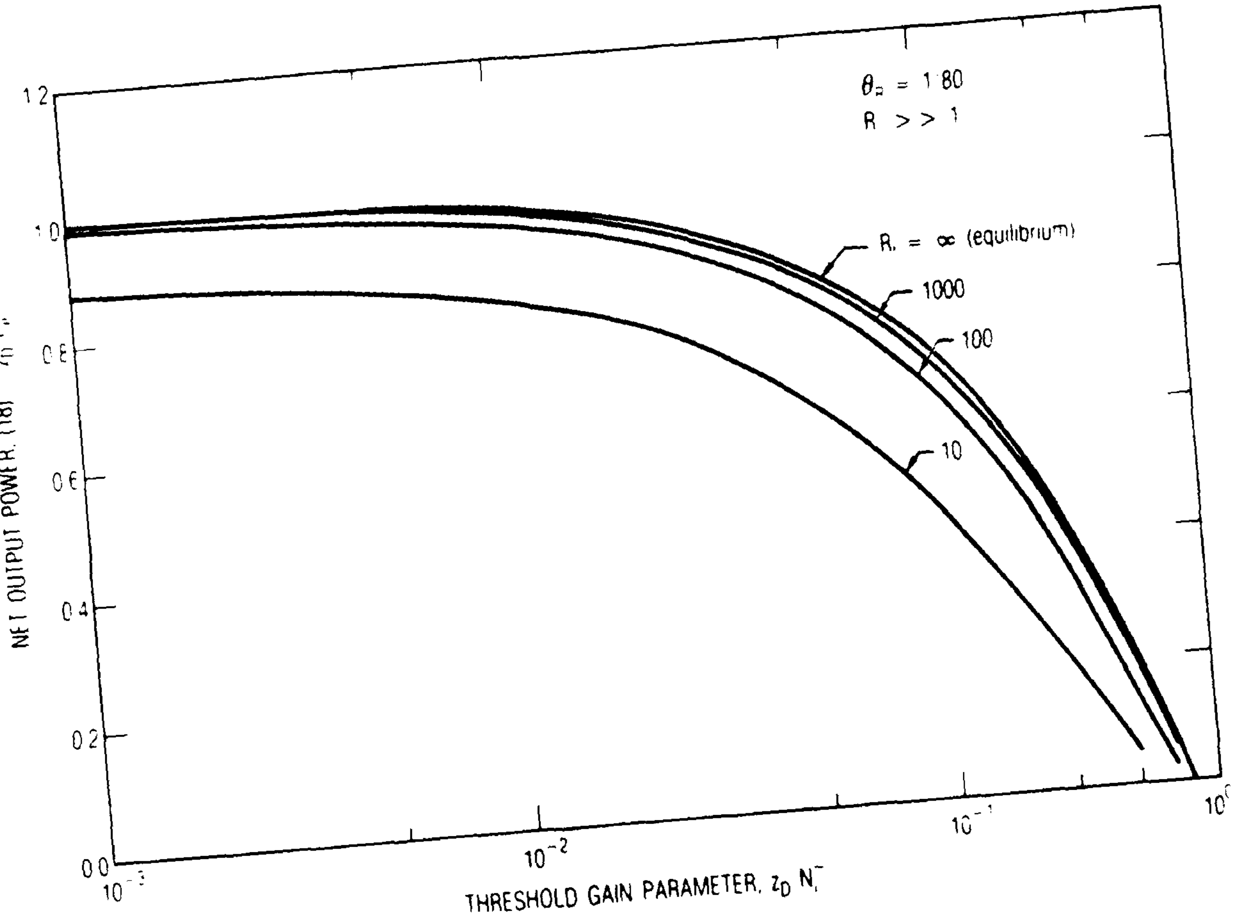

Fig. 8. Variation of Net Output Power with Threshold Gain

The variation of longitudinal mode power $(P_{J,j})_e = \Delta\nu_c[P_J(\nu)]_e$ with frequency is given in Figs. 6a and 6b for $z_i = 0.001$ and 0.01, respectively. These curves are approximately exponential of the form $\exp(-X^2)$ in accord with Eq. (9b). The departure from the exponential form is due to the variation of X_{Jf} with z in Eq. (18a).

Net output power per rotational level $P_{J,e}$ is given in Figs. 7a and 7b. Maximum power is obtained on J = 6 as expected. The variation of $P_{J,e}$ with threshold gain is given in Fig. 7a. Note that the power $P_{6,e}$ increases with increase in threshold gain, reaches a maximum at approximately $(2/\pi)\ Z_d G_c = 0.05$, and then decreases with further increase in threshold gain. The reason for this behavior can be deduced from Figs. 7 and 8. Thus, it is seen from Figs. 7b and 8 that the number of active rotational levels J decreases, while net laser power remains fairly constant, with increase of threshold gain in the region where the threshold gain is small. Hence, for the present cases, the output on lines $3 \leq J \leq 9$ increases, while the output on lines $J < 3$ and $J > 9$ decreases with an initial increase in threshold gain, as indicated in Fig. 7a. When $(2/\pi)\ z_d G_c = 0.05$, the output at each J level, as well as the number of active J levels, both decrease with further increase in $(2/\pi) z_d G_c$.

Figure 8 indicates the effect of threshold gain and translational relaxation rate on net output power. When $(2/\pi) z_D G_c \lesssim 0.05$, the results for the realistic value $R_t = 100$ agree within about 5% with those for translational equilibrium $(R_t \to \infty)$. Hence equilibrium solutions tend to provide realistic estimates for net output power from cw chemical lasers operating under saturated conditions.

The corresponding case of rotational nonequilibrium and translational equilibrium is discussed in Appendix C. The latter is a common assumption.[3,4,5] In this case, there is a single longitudinal mode, at line center, for each rotational energy level with sufficient gain to lase. The output from each rotational level, and the net output power, are indicated in Fig. 9 and Table III, respectively. The output is intermediate between the case of rotational and translational equilibrium and the case of rota-

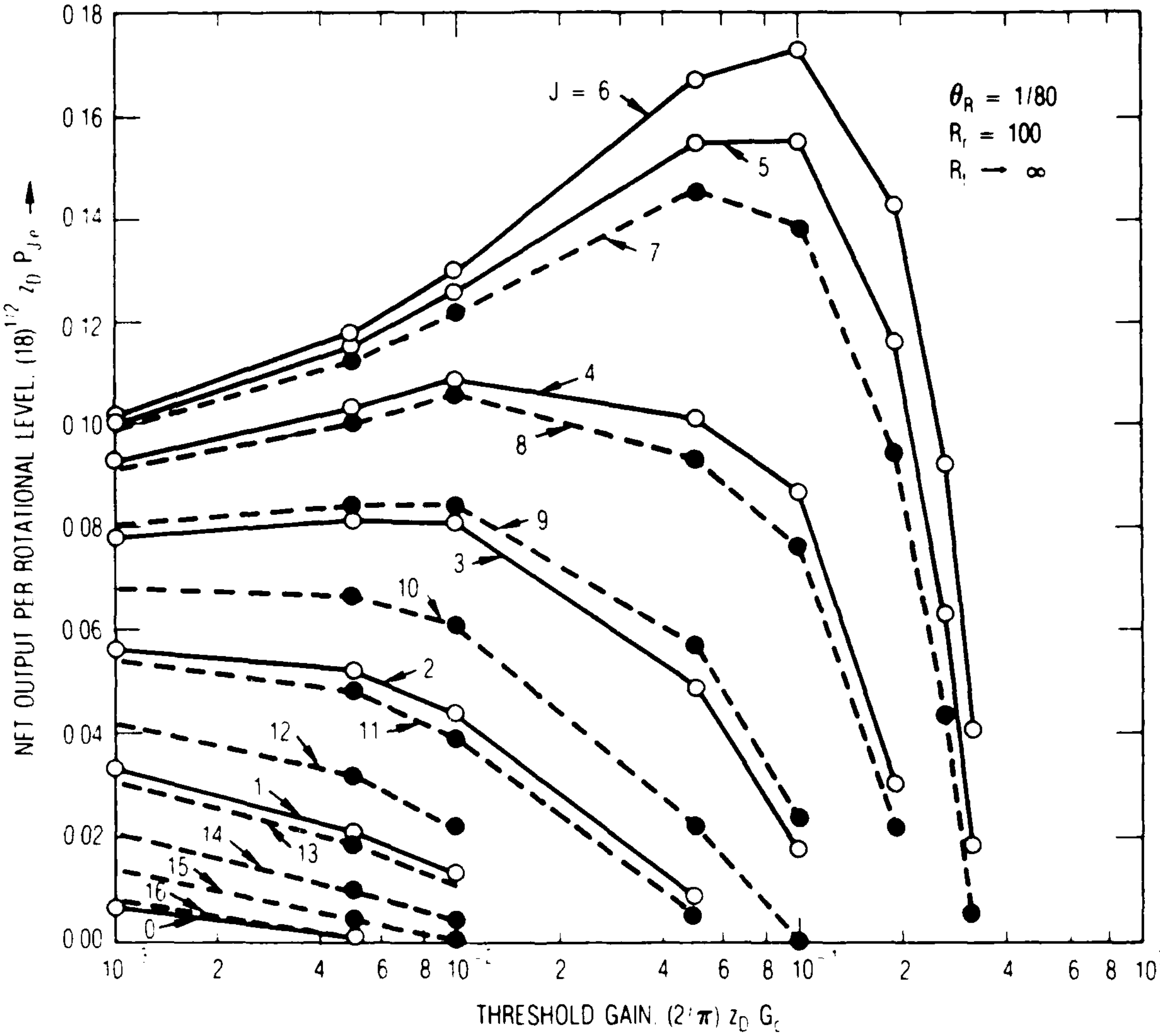

Fig. 9. Net Output Power from Each Rotational Level for Case of Translational Equilibrium and Rotational Nonequilibrium [Eq. (C-3)]

TABLE III. Net output power for cw chemical laser with laminar mixing, $\theta_R = 1/80$, and (a) translational and rotational èquilibrium, (b) translational equilibrium and rotational nonequilibrium, or (c) translational and rotational nonequilibrium with $\Delta\nu_c << \Delta\nu_h << \Delta\nu_d$.

zi	Net Output Power, $(18)^{1/2} z_D P_e$		
	(a) $R_r \to \infty$ $R_t \to \infty$	(b) $R_r = 100$ $R_t \to \infty$	(c) $R_r >> 1$ $R_t = 100$
0.001	0.997	0.986	0.984
0.005	0.984	0.871	0.965
0.010	0.968	0.953	0.945
0.050	0.843	0.822	0.800
0.100	0.694	0.671	0.639
0.200	0.427	0.405	0.363
0.300	0.218	0.199	0.156
0.400	0.077	0.063	0.033
0.500	0.009	0.004	0.000
0.552	0.000	0.000	0.000

tional and translational nonequilibrium. The differences become more pronounced as the degree of saturation is decreased.

IV. CONCLUDING REMARKS

The present model provides an improvement over previous models (e.g., Refs. 3 to 8) because multiple longitudinal modes, as well as multiple rotational laser levels, are included. Although the present development assumes an F-P resonator, it is expected that the results characterize the performance of cw chemical lasers with more realistic resonator configurations.

A comparison between the present model and a detailed numerical code calculation,[10,11] presented in Ref. 7, suggests that Eq. (3c) is overly restrictive and that the present model provides reasonable results for $\Delta\nu_c/\Delta\nu_h = 0(1)$ (e.g., $p = 10$ Torr, $L = 10$ m).

APPENDIX A. PARTIAL LIST OF SYMBOLS

c	speed of light in vacuum
$D(\,)$	Dawson integral, Eq. (12d)
$\bar{f}_J$	fraction of particles in rotational energy level, Eq. (B-4d)
$\bar{f}_r$	reference value of $\bar{f}_J$, Eq. (B-4d)
f_J	$\bar{f}_J/\bar{f}_r$
G_c	normalized threshold gain, Eq. (B-5d)
$G_J(\nu)$	normalized gain, Eq. (B-5b)
$g_J(\nu)$	gain, Eq. (B-5a)
$\bar{I}_{J,j}$	intensity for longitudinal mode J,j
$\bar{I}_J, \bar{I}$	net intensities
$\bar{I}_J(\nu)$	intensity per unit ν, Eq. (6)
$I_{J,j}$	nondimensional intensity, Eq. (B-6a)
J	rotational energy level
j	longitudinal mode number
k_{cd}, k_{tr}, k_{rr}	deactivation, translational and rotational relaxation rates, Ref. 12
$L(\nu-\nu')$	Lorentzian distribution, Eq. (B-5a)
$N^-_{J\nu}, N^-_J, N^-$	normalized inversion number densities, Eq. (B-3)
N_T	normalized total number of lasing species, Eq. (B-3)
$n_v(J,\nu), n_v(J), n_v$	particle number densities, Eq. (B-3)
n_T	total number of lasing species, $n_1 + n_2$
n_r	reference value for n_2
$P_J(\nu), P_J, P$	normalized output power released up to station ζ, Eqs. (10) and (B-6c)
$[P_J(\nu)]_e, P_{J,e}, P_e$	net output power released between stations ζ_i and ζ_e, Eqs. (10) and (B-6c)
$\bar{p}_o$	reciprocal Doppler width, Eq. (B-4d)
R_m	Fabry-Perot resonator mirror reflectivity
R_t, R_r	collisional rate ratios, k_{tr}/k_{cd}, k_{rr}/k_{cd}
S	parameter, Eq. (B-6c)
T	temperature

APPENDIX A. PARTIAL LIST OF SYMBOLS (continued)

T_R	characteristic rotational energy temperature, which equals 30.16K for HF, Eq. (B-4d)
u	streamwise velocity, Fig. 1a
v	vibrational energy level
v_y	thermal velocity in y direction, Fig. 1a
X	normalized frequency, Eq. (B-4c)
X_{Jf}	value of X corresponding to largest active longitudinal mode frequency $\nu_{J,f}$, Figs. 2 and 4b
x	streamwise distance, Fig. 1a
x_D	characteristic diffusion distance, Fig. 1a
y	transverse distance, Fig. 1a
y_f	flame sheet ordinate, Fig. 1b
z	$\zeta^{1/2}$
z_D	$\zeta_D^{1/2}$
ϵ_r	energy per mole of photons
ζ	normalized streamwise distance, $k_{cd}\, x/u$
ζ_D	normalized diffusion distance, $k_{cd}\, x_D/u$
θ_R	characteristic rotational temperature parameter, T_R/T
λ	wavelength
ν	frequency
$\nu_{J,j}$	longitudinal mode frequency
ν_o	line center frequency
$\Delta\nu_d$	Doppler width [full-width, half-maximum (FWHM)]
$\Delta\nu_h$	homogeneous width (FWHM)
$\Delta\nu_c$	longitudinal mode separation, c/2L
$\bar{\sigma}_r$	cross section for stimulated emission, Eq. (B-5a)
ϕ_t, ϕ_r	parameters, Eqs. (12b) and (C-1f)

Subscripts

e	end of lasing region
i	start of lasing region
J	rotational level
j	longitudinal mode
m	maximum value
r	reference value or rotational relaxation value
v	vibrational level

Superscripts

(+),(-)	radiation in +y, -y directions
-	difference of number densities, Eq. (B-3)

APPENDIX B. NONDIMENSIONAL VARIABLES

Geometry

$$y/w = (x/x_D)^{1/2} \quad \text{Laminar Flame Sheet} \tag{B-1}$$

$$\zeta = k_{cd}\, x/u; \qquad \zeta_D = k_{cd}\, x_D/u \tag{B-2}$$

Number Density

$$N^-_{J\nu} = \frac{[n_2(J,\nu) - n_1(J,\nu)]y_f}{n_r w\, \bar{f}_r\, \bar{p}_o} \tag{B-3a}$$

$$N^-_J = \frac{[n_2(J) - n_1(J)]y_f}{n_r w\, \bar{f}_r} \tag{B-3b}$$

$$N^- = (n_2 - n_1)y_f/(n_r w) \tag{B-3c}$$

$$N_T = (n_2 + n_1)y_f/(n_r w) = n_T y_f/(n_r w) \tag{B-3d}$$

Equilibrium Number Density Distributions

$$\frac{n_v(J,\nu)}{n_v(J)} = \bar{p}_o\, e^{-X^2} \quad \text{Translational Equilibrium} \tag{B-4a}$$

$$\bar{p}_o = \left(\frac{4\ln 2}{\pi}\right)^{1/2} / \Delta\nu_d \tag{B-4b}$$

$$X = (4\ln 2)^{1/2}\, (\nu - \nu_o)/\Delta\nu_d \tag{B-4c}$$

$$\frac{n_v(J)}{n_v} = \bar{f}_J = \frac{(2J + 1)\exp[-J(J + 1)\theta_R]}{\sum_J (2J + 1)\exp[-J(J + 1)\theta_R]} \qquad \text{(B-4d)}$$

$$= \bar{f}_r f_J \qquad \text{Rotational Equilibrium}$$

Gain

$$g_J(\nu') = \bar{\sigma}_r \int_{-\infty}^{\infty} [n_2(J,\nu) - n_1(J,\nu)]\, L(\nu - \nu')d\nu \quad \text{Q-Branch} \qquad \text{(B-5a)}$$

$$L(\lambda - \lambda') = \left\{1 + 4\left[(\nu - \nu')/\Delta\nu_h\right]^2\right\}^{-1}$$

$$G_J(\nu') = g_J(\nu')\; y_f/(n_r w\; \bar{f}_r \bar{p}_o\; \Delta\nu_h\; \bar{\sigma}_r)$$

$$= \int_{-\infty}^{\infty} \bar{N}_{J\nu}\; L(\nu - \nu')d\nu/(\Delta\nu_h) \qquad \text{(B-5b)}$$

$$g_c = (-\ell n\; R_m)/(y_f n_{sc}) \qquad \text{Threshold Gain} \qquad \text{(B-5c)}$$

$$G_c = g_c y_f/(n_r w\; \bar{f}_r \bar{p}_o\; \Delta\nu_h\; \bar{\sigma}_r) \qquad \text{(B-5d)}$$

Intensity and Power

$$I_{J,j} = \bar{I}_{J,j} / [\varepsilon_r k_{tr} / (2\bar{\sigma}_r)] \tag{B-6a}$$

$$I = \sum_J I_J = \sum_J \sum_j I_{J,j} \tag{B-6b}$$

$$P = \frac{\bar{P}}{n_r w\, u \varepsilon_f} = \frac{S\, G_c}{2\pi} \int_{\zeta_i}^{\zeta} I d\zeta$$

$$S = \pi \bar{p}_o\, \bar{f}_r\, R_t\, \Delta\nu_h \tag{B-6c}$$

Rates

$$R_t = \frac{k_{tr}}{k_{cd}} \; ; \; R_r = \frac{k_{rr}}{k_{cd}} \tag{B-7}$$

APPENDIX C

ROTATIONAL NONEQUILIBRIUM AND TRANSLATIONAL EQUILIBRIUM

We now consider the case of rotational nonequilibrium and translational equilibrium ($R_t \to \infty$) but assume $R_r >> 1$. In this limit, there is a single longitudinal mode at line center for each rotational energy level J that can maintain threshold gain.

The assumption $R_t \to \infty$ implies an equilibrium line shape

$$N^-_{J\nu} = e^{-X^2} N^-_J \qquad \text{(C-1a)}$$

that replaces Eq. (4a) due to violation of Eq. (3d). Assuming $\Delta\nu_h << \Delta\nu_d$, the gain, from Eq. (4c), is

$$(2/\pi)\ G_J(\nu) = e^{-X^2}\ N^-_J$$

The relation between threshold gain G_c and rotational number density N^-_J, for those rotational energy levels that can support a single longitudinal mode at line center, is

$$(2/\pi)G_c = N^-_J \qquad \text{(C-1b)}$$

For the case of laminar mixing, Eqs. (4b) and (4d) become, respectively,

$$z_D \frac{dN^-}{dz} = 1 - 2zz_D N^- - 2z^2 - 2z\phi_r \sum_J (\pi \ell n2)^{1/2} \frac{\Delta\nu_h}{\Delta\nu_d} \frac{R_t}{R_r} I_J \qquad \text{(C-1c)}$$

$$(\pi \ell n2)^{1/2} \frac{\Delta\nu_h}{\Delta\nu_d} \frac{R_t}{R_r} I_J = \frac{f_J}{f_{J,m}} \frac{N^-}{N^-_i} - 1 \geq 0 \qquad \text{(C-1d)}$$

where

$$z_d N_i^- = (2/\pi) z_D G_c / f_{J,m} = 2D(z_i) - z_i \qquad \text{(C-1e)}$$

$$\phi_r = \phi_t (R_r / R_t) \qquad \text{(C-1f)}$$

Eq. (C-1c) can be integrated upon specification of z_i, θ_R, $\bar{f}_r$, and R_r. The summation in Eq. (C-1c) is evaluated using Eq. (C-1d) and includes those values of J for which Eq. (C-1d) is nonnegative. Net output power from each rotational transition and net laser power are found from

$$z_D P_{J,e} = \phi_r \int_{z_i}^{z_e} (\pi \ln 2)^{1/2} \frac{\Delta\nu_h}{\Delta\nu_d} \frac{R_t}{R_r} I_J \, z dz \qquad \text{(C-2a)}$$

$$z_D P_e = \sum_J z_D P_{J,e} \qquad \text{(C-2b)}$$

Numerical results are presented in Table III and Fig. 9 for the case

$$\begin{aligned} z_i &= 0.001 - 0.5 \\ \theta_R &= 1/80 \qquad (J_m = 6) \\ \bar{f}_r &= 0.0957 \qquad (f_{J,m} = 1) \qquad \text{(C-3)} \\ R_r &= 100 \\ R_t &\to \infty \end{aligned}$$

REFERENCES

1. H. Mirels, R. Hofland, and W. S. King, "Simplified Model of CW Diffusion Type Chemical Laser," AIAA J. 11, (12), 156-164 (February 1973).

2. G. Emanuel, "Numerical Modeling of Chemical Lasers," Handbook of Chemical Lasers," edited by R.W.F. Gross and J. F. Bott (John Wiley and Sons, 1976), pp. 488-496.

3. R. J. Hall, "Rotational Nonequilibrium and Line-Selected Operation in cw DF Chemical Lasers," IEEE J. of Quantum Electron. QE-12, 453-462 (August 1976).

4. L. H. Sentman and W. Rushmore, "Computationally Efficient, Rotational Nonequilibrium cw Chemical Laser Model," AIAA J. 19 (10), 1323 (October 1981).

5. T. T. Yang, "Modeling of cw HF Chemical Laser with Rotational Nonequilibrium," J. de Phys. Colloque C9 41 (11), C9-51 (November 1980).

6. H. Mirels, "Inhomogeneous Broadening Effects in cw Chemical Lasers," AIAA J. 17 (5), 478-489 (May 1979).

7. H. Mirels, "Inhomogeneous Broadening Effects in Multimode cw Chemical Lasers," Appl. Opt. 20 (2), 362-373 (15 January 1981).

8. H. Mirels, "Multimode Low Pressure cw Chemical Laser Performance Including Source Flow Effects," Appl. Opt. 20 (14), 2379-2388 (15 July 1981).

9. A. A. Stepanov and V. A. Shcheglov, "Dynamic Saturation of Optical Transitions in High Power Molecular Lasers," Soviet J. Quantum Electron. 12 (5), 619-624 (May 1982).

10. D. L. Bullock, M. M. Valley, and R. S. Lipkis, Advanced Chemical Laser Optics Study, Final Report, Contract No. F29601-79-C-0011 (TRW, 15 July 1982).

11. D. L. Bullock, J. de Phys. C9 37 (1980).

12. H. Mirels, "Effects of Translational and Rotational Nonequilibrium on cw Chemical Laser Performance," Appl. Opt. (1 January 1988).

13. M. Abramowitz and I. A. Stegun, Handbook of Mathematical Functions, AMS 55 (National Bureau of Standards, June 1964), pp. 297-303.

LABORATORY OPERATIONS

The Aerospace Corporation functions as an "architect-engineer" for national security projects, specializing in advanced military space systems. Providing research support, the corporation's Laboratory Operations conducts experimental and theoretical investigations that focus on the application of scientific and technical advances to such systems. Vital to the success of these investigations is the technical staff's wide-ranging expertise and its ability to stay current with new developments. This expertise is enhanced by a research program aimed at dealing with the many problems associated with rapidly evolving space systems. Contributing their capabilities to the research effort are these individual laboratories:

Aerophysics Laboratory: Launch vehicle and reentry fluid mechanics, heat transfer and flight dynamics; chemical and electric propulsion, propellant chemistry, chemical dynamics, environmental chemistry, trace detection; spacecraft structural mechanics, contamination, thermal and structural control; high temperature thermomechanics, gas kinetics and radiation; cw and pulsed chemical and excimer laser development including chemical kinetics, spectroscopy, optical resonators, beam control, atmospheric propagation, laser effects and countermeasures.

Chemistry and Physics Laboratory: Atmospheric chemical reactions, atmospheric optics, light scattering, state-specific chemical reactions and radiative signatures of missile plumes, sensor out-of-field-of-view rejection, applied laser spectroscopy, laser chemistry, laser optoelectronics, solar cell physics, battery electrochemistry, space vacuum and radiation effects on materials, lubrication and surface phenomena, thermionic emission, photosensitive materials and detectors, atomic frequency standards, and environmental chemistry.

Computer Science Laboratory: Program verification, program translation, performance-sensitive system design, distributed architectures for spaceborne computers, fault-tolerant computer systems, artificial intelligence, microelectronics applications, communication protocols, and computer security.

Electronics Research Laboratory: Microelectronics, solid-state device physics, compound semiconductors, radiation hardening; electro-optics, quantum electronics, solid-state lasers, optical propagation and communications; microwave semiconductor devices, microwave/millimeter wave measurements, diagnostics and radiometry, microwave/millimeter wave thermionic devices; atomic time and frequency standards; antennas, rf systems, electromagnetic propagation phenomena, space communication systems.

Materials Sciences Laboratory: Development of new materials: metals, alloys, ceramics, polymers and their composites, and new forms of carbon; nondestructive evaluation, component failure analysis and reliability; fracture mechanics and stress corrosion; analysis and evaluation of materials at cryogenic and elevated temperatures as well as in space and enemy-induced environments.

Space Sciences Laboratory: Magnetospheric, auroral and cosmic ray physics, wave-particle interactions, magnetospheric plasma waves; atmospheric and ionospheric physics, density and composition of the upper atmosphere, remote sensing using atmospheric radiation; solar physics, infrared astronomy, infrared signature analysis; effects of solar activity, magnetic storms and nuclear explosions on the earth's atmosphere, ionosphere and magnetosphere; effects of electromagnetic and particulate radiations on space systems; space instrumentation.